Check for updates

Production of value-added chemicals and fuels from selective conversion of C=O, C=C, and C–O bonds in 5-hydroxymethylfurfural over bimetallic catalysts

Xinluona Su,[a,b] Tingting Xiao,[a,b,c] Qihang Gong,[a,b,c] Haiyang Cheng [ID] *[a,b,c] and Fengyu Zhao [ID] *[a,b,c]

The catalytic conversion of biomass-derived 5-hydroxymethylfurfural (HMF) has been extensively studied due to its potential to produce a range of valuable chemicals and fuels through the selective hydrogenation/hydrodeoxygenation of C=O, C=C or C–O bonds. This research has primarily focused on improving reaction rates and controlling product selectivity by designing highly efficient heterogeneous catalysts. It is well established that the catalytic activity and selectivity strongly depend on the electronic and geometric structures of the active species of metal-supported catalysts. These structural features play a critical role in governing the adsorption and activation of reactants and H$_2$ molecules during reactions. This paper provides a comprehensive review of recent advancements in HMF conversion over the past decades, with a particular emphasis on elucidating the catalytic mechanisms of bimetallic catalysts. The key factors, which influence the selective activation of C=O, C=C and C–O bonds, such as the electronic interactions of active metal species (including bimetallic alloys and intermetallic compounds), the structural interactions of active species with the support (encapsulation, metal–N(S) species and oxygen vacancies), and surface acidity (originating from doped secondary metals or inherent acidity of the supports), will be systematically discussed and summarized.

Green foundation

1. This review highlights the utilization of bimetallic catalysts in the selective catalytic hydrogenation of 5-hydroxymethylfurfural. The characteristics, advantages and challenges of bimetallic catalysts in catalyzing 5-hydroxymethylfurfural to value-added chemicals are presented based on the achievements published in these decades.

2. The present review provides concise viewpoints and details on the metal–support interactions, such as the electronic and steric effects, oxygen vacancies, and acidity caused by doping of the second element. These issues are particularly important in the conversion of biomass and catalysis.

3. The utilization of bimetallic catalysts in the selective catalytic hydrogenation of biomass not only reduces energy consumption but also enhances catalyst stability, thereby mitigating the environmental impact caused by discarded catalysts. Developing highly efficient non-precious metals with long lifetimes remains a huge challenge to meet the demands of industrial applications.

Introduction

Biomass is the most promising renewable energy source due to its renewability, abundance, cost-effectiveness, global availability, and potential to partially replace fossil fuels while reducing environmental pollution.[1,2] From an energy perspective, the global total biomass has a potential production capacity of 3.3×10^{18} kJ, which is equivalent to over 80 times the annual energy consumption of the world.[3,4] Notably, renewable resources account for nearly 18% of global energy consumption, of which 72.3% is contributed by biomass until 2018.[4] Considering environmental protection, biomass stands as a powerful renewable energy source and a highly desirable fuel that is close to carbon dioxide neutral.[5] In recent years, with the progress of green energy technology and the heightened global awareness towards environmental conservation, the potential of biomass in industrial application has been further

*[a]State Key Laboratory of Electroanalytical Chemistry, Changchun Institute of Applied Chemistry, Chinese Academy of Sciences, Changchun 130022, PR China.
E-mail: hycyl@ciac.ac.cn, zhaofy@ciac.ac.cn*
[b]Jilin Province Key Laboratory of Green Chemistry and Process, Changchun Institute of Applied Chemistry, Chinese Academy of Sciences, Changchun 130022, PR China
[c]University of Science and Technology of China, Hefei, 230026, PR China

propelled.[6,7] Among the valuable chemicals derived from biomass, 5-hydroxymethylfurfural (HMF) occupies a pivotal position as a key furan-based platform compound and serves as a vital bridge connecting petrochemical and lignocellulosic biomass resources.[8] In 2024, the global market of HMF is expected to be EUR 55 million, with a 1.4% compound annual growth rate.[9] It has widespread industrial applications, including the manufacture of eco-friendly polymers, resins, fuel additives, and intermediates of pharmaceuticals.[10]

The coexistence of three kinds of functional groups of C=O, C–O and a furan ring in the molecule of HMF makes it undergo various reactions such as hydrogenation,[11] hydrogenolysis,[12] amination,[13] etherification,[14] oxidation,[15] ring opening,[16] *etc*. As a result, numerous kinds of chemicals can be produced from HMF (Fig. 1), to meet the diverse demands for the value-added chemicals of market. For example, the selective catalytic hydrogenation of C=O and C–O bonds and the furan ring of HMF can yield 2,5-bis(hydroxymethyl)lfuran (BHMF), 2,5-bis(hydroxymethyl) tetrahydrofuran (BHMTHF), 2,5-dimethylfuran (DMF), 2,5-dimethyltetrahydrofuran (DMTHF), 1,2,6-hexanetriol (1,2,6-HTO), and 1,2-hexanediol (1,2-HDO). DMF and DMTHF are highly promising renewable liquid fuel candidates as their properties are similar to those of commercial gasoline and they are more conducive to storage and transportation.[17] DMF has exceptional characteristics and multiple benefits, including low volatility (with a boiling point of 92–94 °C), high octane number (119), superior energy density (31.5 MJ L^{-1}), minimal energy consumption for separation, and immiscibility with water, making it an ideal liquid biofuel.[18] In addition, DMF can also be applied in semiconductor manufacturing, the pharmaceutical industry and the production of engineering polymers.[19] DMTHF serves as a valuable organic solvent and renewable feedstock for the production of valuable chemicals, such as 2,4-hexadiene that enables new route towards bio-polymers.[20] 1,2,6-HTO and 1,2-HDO are predominantly utilized as a monomer for polyesters and polyurethanes.[8,21] Furthermore, some chemicals produced from HMF can serve as a moisturizing agent, coating, polymer cross-linker, adhesive and high-quality organic solvent.[21,22] Therefore, the catalytic hydrogenation of HMF has attracted much attention and been well studied.[23–26]

The reaction pathway for catalytic hydrogenation of HMF to valuable chemicals containing furan derivatives or aliphatic polyols is illustrated in Fig. 2. The most reported and accepted pathway involves two routes: one way is firstly going through hydrogenation of C=O in HMF to produce BHMF, subsequently, hydrogenolysis of the C–O group to form MFA or hydrogenation of the furan ring to form BHMTHF, and further hydrogenation of the furan ring to give DMTHF; the other way is firstly going through hydrogenolysis of one C–O group to form MF and then hydrogenation of C=O to form MFA, which is ultimately followed by hydrogenolysis of another C–O to form DMF and further hydrogenation of the furan ring to produce DMTHF. Subsequently, BHMF or BHMTHF undergoes ring-opening hydrogenolysis to yield 1,2,6-HTO, or 1,2-HDO, followed by further hydrodeoxygenation. Several kinds of reactions (hydrogenation of C=O, hydrogenation of the furan ring and hydrogenolysis of C–O) are involved in the catalytic conversion of HMF, in which the hydrogenation of the C=O group is the first and important step. When a reactant contains multiple reducible functional groups, selective catalysis becomes crucial in determining the desired product, directly influencing reaction efficiency and atom economy. Consequently, significant research efforts have been dedicated to controlling selectivity by designing efficient heterogeneous catalysts through modulation of the electronic properties and geometric structure of metal active sites. However, challenges remain due to the limited understanding of the interactions between active sites and substrate functional groups. The hydrodeoxygenation of HMF demands coordinated catalysis of multiple active sites, as the high bond energy of C–O poses a substantial kinetic barrier. Most studies have thus focused on developing highly efficient catalysts to lower the activation energy of C–O cleavage with notable progress achieved in recent years.[24,27–29]

Bimetallic catalysts have gained significant attention due to their superior catalytic efficiencies compared to monometallic catalysts. The incorporation of a second metal or metal oxide can significantly alter the catalytic performance such as
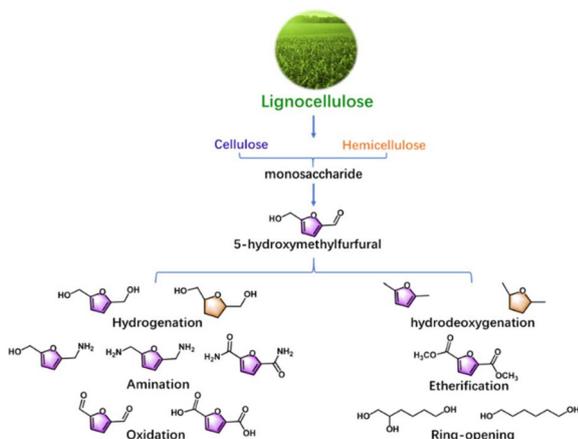

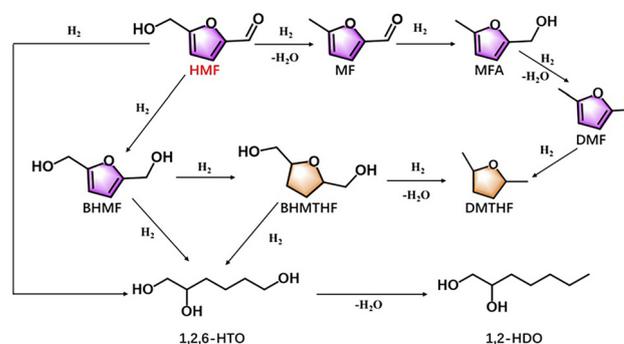**Fig. 1** Possible products formed from catalytic conversion.

Fig. 2 Reaction pathway for catalytic conversion of HMF to furan derivatives and aliphatic polyols.

improving the catalytic selectivity through synergistic effects of the two kinds of metals or other active sites. This review will summarize and evaluate the advancements in the hydrogenation of HMF over the bimetallic catalysts reported in the past decades and discuss the catalytic performances of bimetallic heterogeneous catalysts, such as the activity, selectivity and the catalytic mechanism. In particular, the electronic structure, geometric structure of active metal species and the surface acidity, modulated by doping a second metal, will be considered and reviewed; an informative and profound perspective will also be given.

Bimetallic catalysts

The incorporation of a second metal has emerged as a highly effective strategy to improve the catalytic efficiency of a monometallic catalyst. The promoting effects of doping a second metal will bring electronic and geometric modification of the primary active metal species, as well as modulate the synergistic effects of the active species and the surface acid–base sites. The electronic effects refer to the phenomenon wherein the incorporation of a metal promoter interacts with the primary active metal species through electron transfer between them. Geometric effects refer to the incorporation of a metal promoter that can lead to changes in the geometry or dimension of the primary metal particles. Synergistic effects occur when both the metal species participate in the chemical bonding with the intermediate/transition state, or when the metallic species cooperate with the surface acid or base sites. Thus, the activity and selectivity are improved by the doped metal; particularly, the stability is improved by inhibiting the aggregation of metal particles and/or prohibiting the formation of carbonaceous deposits. The results reported for hydrogenation of HMF on the bimetallic catalysts in this decade are summarized in Table 1. As can be seen in Table 1, Pd-, Pt-, Cu-, and Ni-based bimetallic catalysts are the most extensively studied catalysts for the catalytic conversion of HMF. In most cases, bimetallic catalysts demonstrate superior performance compared to their monometallic counterparts, not only in terms of activity and selectivity but also in terms of stability of the catalyst. For example, monometallic Pt or Pd catalysts often exhibit excessive hydrogenation activity, leading to over-hydrogenated byproducts. When a second metal, particularly non-noble metals, such as Co or Cu is introduced, the electronic state of the primary active metal species can be modified, which alters the adsorption behavior of the substrate, thereby steering the reaction pathway and enhancing selectivity toward the desired products. Furthermore, the incorporation of a second metal can reshape the morphology and geometric structure of the active metal particles, further improving catalytic performance, particularly in terms of stability.

Moreover, non-noble bimetallic catalysts have attracted significant interest due to their low cost and catalytic activity comparable to that of noble metals in the conversion of HMF. Among the most studied non-noble metals, Ni, Cu, and Co-based bimetallic catalysts are widely investigated, while Zn-based catalysts are less frequently studied. Ni- or Cu-based catalysts exhibit high activity for the hydrogenation of C=O bonds in HMF; the introduction of a second metal (e.g., W, Ce, Re, Co, or Fe into Ni, or Fe, Co, Mg or Ni into Cu) can further enhance their performance by promoting the hydrogenation of C=C bonds and facilitating C–O bond cleavage. This modification adjusts the adsorption configuration of HMF, thereby influencing product distribution by improving hydrogenation or hydrogenolysis reactions. Additionally, the incorporation of a second metal can lead to the formation of protective surface layers, such as metal oxide or carbon coatings (e.g., core–shell structure), which significantly enhance catalyst stability.

Therefore, introducing a second metal dopant can enhance catalytic performance by modulating the electronic structure and geometry of the primary active metal species, as well as tuning surface acidity through strong metal–support interactions. The interactions will promote the formation of bimetallic alloys or intermetallic compounds, generate new acid and oxygen vacancy, create additional active species, and may even lead to the development of coating layers. This review summarizes and discusses these critical aspects of bimetallic catalysts in the catalytic conversion of HMF.

Besides, the reaction conditions such as temperature and solvent strongly influence the reaction results. The hydrogenation of the C=O bond in HMF can be performed at relatively low temperatures, while the hydrodeoxygenation of the C–O bond requires a relatively high temperature. As for hydrogenation of HMF, the polar protic solvents (water, methanol, ethanol, THF, 1,4-dioxane, etc.) are more efficient, among which water and ethanol are the most effective solvents for catalytic conversion of HMF due to their ability to modulate the reaction mechanism by altering the substrate's adsorption, activation, and desorption processes.[30–32] Moreover, water and ethanol in some cases serves as hydrogen donors, furnishing hydrogen atoms during the reaction, which not only mitigates the necessity for high hydrogen pressure but also contributes to the improvement of reaction efficiency.[33–37] The solvent effects will not be involved or reviewed in this paper.

Electronic interactions

In most cases, bimetallic catalysts exhibit strong interactions due to electron transfer between the constituent metals, which occur through the formation of metallic alloys or intermetallic compounds. Electron transfer in metallic alloys depends on electronegativity differences and Fermi level alignment. If metal A has a higher electronegativity than metal B, it will attract electrons more strongly, leading to partial electron transfer from metal B to A. Thus, the catalytic activity and selectivity are modified by incorporating the second metal species, as the d-band electronic structure of primary metal species controls the adsorption strength of the reactant and the intermediate. Herein, bimetallic alloys and intermetallic compounds formed by doping a second metal species, thereby improving the catalytic performance in HMF conversion, will be reviewed.

Table 1 Selected results for conversion of HMF on the bimetallic catalysts reported in this decade

Catalyst	H_2 (MPa)	T (°C)	Time (h)	Solvent[a]	Conv. (%)	Yield (%)	Product	Ref.
PdRu/RGO	1	20	6	H_2O	99.9	92.9	BHMTHF	38
PdAu/C	0.1	60	12	THF	>99	96	DMF	39
PdAu$_4$/GC800	1	150	4	THF	86.8	81.9	DMF	40
Pd–Cu@C	1.5	150	7	THF	100	96.5	DMF	41
PdCu/AC-BCC	4	30	20	THF	>99	93.6	DMF	42
Pd–Cu/RGO	3	200	2	i-PrOH	96	95	DMF	33
PdCu@DABs	1.5	130	10	THF	100	98	DMF	43
PdCu/BCN	1.5	180	4	THF	100	99.2	DMF	44
PdZn	1.5	180	10	DIOX	100	98.7	BHMF	45
Pd/Zn/C	0.8	150	8	THF	99	84	DMF	46
PdCo/AZMO	1	100	2	THF	>99	97	DMF	47
Pd$_{0.5}$Co$_{10}$/MoC$_x$	2	180	8	THF	99.9	97	DMF	48
Pd–Co–CoOx@NC	1.5	180	2	DIOX	100	97.8	DMF	49
Pd–Co$_9$S$_8$/S-CNT	0.3	120	13	THF	96	80.4	DMF	50
PdNi/SBA-15	1	140	5	DIOX	100	96	BHMTHF	51
Pd–Fe/C	2	150	3	THF	100	85	DMF	52
PtIr-CMK-3	1.5	120	4	THF	98	86	DMF	53
Pt$_3$Sn$_1$/g-C$_3$N$_4$	2	80	1	H_2O	99.1	97.2	BHMF	54
Pt$_3$Sn/SnO$_2$/rGO	2	70	0.5	EtOH	>99	>98	BHMF	55
Pt$_3$Co$_2$/C	3.3	160	—	n-PrOH	100	98	DMF	56
Pt$_3$Co-1.2	1	120	2	n-BuOH	>99	100	DMF	57
Pt/Co/MWCNTs	1	160	8	n-BuOH	100	92.3	DMF	58
Pt$_3$Co/BNNs	1	160	24	EtOH	100	78	DMF	59
PtCo/Al$_2$O$_3$	2	40	2	—	100	99.9	BHMF	60
PtCo/Al$_2$O$_3$	2	160	2	—	100	86.7	DMF	60
PtCo@HCS	1	180	2	n-BuOH	100	98	DMF	61
PtCo/LOC	1	120	3.5	H_2O-THF	100	79.8	1,2,6-HTO	37
PtCo/CeO$_2$	3	135	24	H_2O	100	42	1,2,6-HTO	62
PtCo/CeO$_2$	1	120	2	H_2O	80	40.2	1,2,6-HTO	36
PtNi/SBA-15	1.5	30	2	H_2O	83.3	68.2	BHMF	63
Pt/Ni@C	3	100	1	H_2O	100	99	BHMF	64
PtFe/C	3	180	4	DIOX -H_2O	100	99.6	DMF	65
Pt–FeOx/AC	1.5	180	6	n-BuOH	100	91	DMF	66
Ru–Ir/C	1	120	18	THF	100	99	DMF	67
Ru–Co/AC	1	200	1.5	THF	98.7	97.9	DMF	68
Ru–Co/SiO$_2$	1.5	180	2	THF	100	96	DMF	69
RuCo/CoOx	0.5	200	2.5	DIOX	100	96.5	DMF	70
Ru–MoOx/C	1.5	180	1	n-BuOH	100	79.8	DMF	71
Ru–Ni/TiO$_2$	3	160	4	DIOX	100	71	DMF	72
Ag–Cu/Al$_2$O$_3$	1.5	180	6	THF	100	93	DMF	73
Co@CuCo/Al$_2$O$_3$	1	130	10	DIOX	100	91.7	DMF	74
Cu–Co/Al$_2$O$_3$	3	200	8	THF	98	83	DMF	75
Cu–Co/CeOx	1.5	210	8	THF	96.5	91.3	DMF	76
CuCo@C	5	180	8	EtOH	100	99.4	DMF	77
CuCo/NC	1	100	4	THF	93.7	92.4	BHMF	78
Cox–Cu@C	3	160	3	n-PrOH	100	85	DMF	79
CuCo-IG	2	180	4	2-Butanol	100	93.7	DMF	80
CuCoMgAlOx	2	90	5	EtOH	100	95	BHMF	81
K–Cu/Al$_2$O$_3$	2	120	1	EtOH	99.2	98.9	BHMF	82
CuFe@C	1	110	24	MeOH	94	94	BHMF	83
CuAlMo-HTs	3	180	6	H_2O	58.5	55.8	BHMF	84
CuMgAl	6	150	10	i-PrOH	100	42	1,2-HDO	21
NiCu$_3$/C	3.3	180	—	i-PrOH	100	98.7	DMF	85
Cu–Ni/BC	4	220	12	THF	94.6	93.5	DMF	86
Ni–Cu/TCC	1.5	275	23	—	100	67	DMF	86
Ni–Cu/SBA-16	2	210	4	THF	100	60.7	DMF	87
Ni–Cu/TS-1	0.5	180	7	THF	100	97.3	DMF	88
Ni–Cu/ZrO$_2$	1.5	150	5	n-BuOH	83	60	BHMF	89
Ni–Cu/ZrO$_2$	1.5	225	5	n-BuOH	92	65	DMF	89
Cu–Ni/TiO$_2$	2.5	200	8	DIOX	100	84.3	DMF	90
CuNi/HSAG	3	60	2	H_2O	100	99	BHMF	91
Ni–Ir/SiO$_2$	1	58	4	THF	100	69	DMF	92
NiFe/TiO$_2$	3	220	1	DIOX	96	71	DMF	93
Ni–Fe/TiO$_2$	3	220	2	DIOX	100	97	DMF	94
NiFeBOx	1	160	1	EtOH	100	98.9	DMF	95
Ni$_{0.74}$Fe$_{0.97}$Al	4	180	—	EtOH	100	90.5	DMF	96
Ni–Fe/NPCMs	1.9	135	2	MeOH–H_2O	100	93.6	BHMF	97
Ni–Fe/NPCMs	4.8	135	8	MeOH–H_2O	100	94.9	BHMTHF	97
Ni$_{1.5}$GaAl-LDO	3	140	1	Tridecane	100	95.6	BHMF	98

Table 1 *(Contd.)*

Catalyst	H_2 (MPa)	T (°C)	Time (h)	Solvent[a]	Conv. (%)	Yield (%)	Product	Ref.
Ni_1Ga_1	3	120	6	H_2O	100	98.4	BHMF	99
NiZnAl	1.5	180	15	DIOX	100	93.6	DMF	100
$Ni_2In/MgO–Al_2O_3$	2	200	10	THF	100	93.2	DMF	101
$Ni–W_2C/AC$	4	180	3	THF	100	96	DMF	102
$NiRe/TiO_2$	5	40	4	*n*-BuOH–H_2O	97.2	83.3	BHMF	103
$Ni–Ce/Al_2O_3$	5	140	6	THF–H_2O	100	96	BHMF	22
Ni–Mn/AC	2	180	4	THF	100	98.5	DMF	104
NiCoTi	1.5	200	6	THF	90.7	86.9	DMF	105
Co_1Ni_1@C	2	160	15	H_2O	100	91	BHMTHF	106
Co_2Ni_1@NC	2	220	4	EtOH	100	93	DMF	107
NiCoAl	4	120	4	MeOH	100	64.5	1,2,6-HTO	108
Co–FeOx/NC	2	80	6	THF	100	99.9	DMF	109
CoMo@NC	1.5	170	12	*n*-PrOH	95	77	DMF	110
CoCuAl	3	120	3	MeOH	100	72	1,2,6-HTO	111
$Zn_1Co_3/N–C$	1	120	6	THF	100	93.7	BHMF	112
$Zn_1Co_3/N–C$	1	170	6	THF	100	93.5	DMF	112
$ZrO_2–Co/Al_2O_3$	2	150	6	THF	100	97.3	DMF	113

[a] H_2O: water, THF: tetrahydrofuran, *n*-PrOH: *n*-propanol, i-PrOH: i-propanol, DIOX: 1,4-dioxane, EtOH: ethanol, *n*-BuOH: *n*-butanol, and MeOH: methanol.

Bimetallic alloys. A metallic alloy is usually formed by blending and melting two or more metallic elements together at a high temperature by integrating one metal element into the crystal phase of a metallic matrix. This kind of alloy is termed a "nanoalloy"; due to its nanoscale dimensions and numerous defects present at kinks or steps, a nanoalloy exhibits high surface energy and possesses a multitude of active sites. Besides, nanoalloys possess intrinsic characteristics such as a reconfigurable electronic structure, adaptable configurations, and adjustable composition and ratio of metals, and thus they attract much attention in the heterogeneous catalysis. In particular, the bimetallic alloy catalysts have been well studied for the catalytic conversion of HMF. For example, a kind of bimetallic alloy catalyst of PdAu/C was prepared and studied for the conversion of HMF. With compared to Pd/C and Au/C, the PdAu/C was much more efficient in catalyzing the conversion of HMF, producing DMF with a high yield of 96%. The bimetallic alloy of the PdAu phase was confirmed to form with an electron transferring from Pd to Au, forming an electron deficient $Pd^{\delta-}$ and electron rich $Au^{\delta+}$, thus facilitating C–O bond cleavage.[39]

Han *et al.* synthesized a body-centered cubic (BCC) PdCu nanoalloy supported on activated carbon (PdCu/AC-BCC) and a face-centered cubic (FCC) PdCu nanoalloy catalyst (PdCu/AC-FCC) for catalytic conversion of HMF at room temperature. The introduction of Cu into Pd could tune the electronic structure of Pd through the electron transfer from Cu to Pd. They found that the crystallographic phase of PdCu nanoalloys governed the selectivity of HMF conversion. The hydrogenation of the furan ring was the dominating reaction over FCC PdCu nanoalloys with low selectivity toward DMF; while the BCC PdCu nanoalloys exhibited outstanding performance for the hydrodeoxygenation reaction, producing DMF in a yield of 93.6%. Density functional theory (DFT) studies demonstrated that the adsorption modes of HMF are highly sensitive to the microstructure of catalyst surfaces. As noted in Fig. 3, the
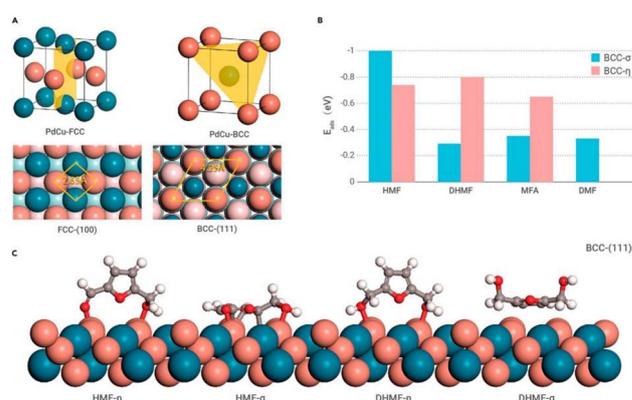

Fig. 3 Furanic adsorption behaviors on PdCu surfaces. (A) Exposed surfaces of PdCu-FCC/BCC considered in DFT calculations. The distances between neighbor top metal atoms are marked. (B) Adsorption energies of HMF, BHMF (note, BHMF is named DHMF within the figure), MFA, and DMF on PdCu-BCC, respectively. (C) Optimized geometries for adsorption configuration of HMF and BHMF on PdCu-BCC. Dark blue, Pd; light blue, sublayer Pd; orange, Cu; pink, sublayer Cu; silver, H; gray, C; and red, O. Reproduced from ref. 42 with permission from Cell Press, copyright (2025).

adsorption of HMF on the PdCu surface involves a η-adsorption mode mainly *via* the oxygenated pendant functions (aldehyde and hydroxyl groups). The η-adsorption mode is predominant on the surface of PdCu/AC-BCC; thus, the hydrodeoxygenation of the C–O group in HMF and its intermediates proceeded smoothly, while the hydrogenation of the furan ring in DMF was almost completely blocked, producing DMF in high yield over the PdCu/AC-BCC catalyst.[42]

Besides, PdCu alloy formation was also reported on the bimetallic catalyst of Cu–Pd@C with electron transferring from Cu to Pd, on which DMF was produced in a yield of 96.5%. The enhanced catalytic performance of Pd upon alloying with Cu by lowering the d-band center of Pd reduces the chemisorp-

tion energy of H_2 on the Pd surface and thereby promotes catalytic hydrogenation.[41] Furthermore, the PdCu alloy was also reported to form on Cu–Pd/RGO,[33] CuPd@DABs,[43] and CuPd/BCN[44] catalysts, producing DMF selectively in yields above 95%.

On the other hand, Pd can form alloys with Co on different supports like Al–Zr mixed oxide and MoCx, forming PdCo/AZMO[47] and PdCo/MoCx catalysts.[48] The synergistic interaction between Pd and Co, combining with the unique properties of the support materials enhances hydrogen dissociation, facilitates C–O bond cleavage and improves the overall efficiency of the reaction. Thus, all these catalysts exhibited remarkable catalytic performance in the selective hydrogenation of HMF to DMF with a yield above 97%. For the PdCo/MoCx catalyst, the increased β-Mo_2C phase could promote charge transfer from the support to the Pd–Co bimetallic site, facilitating the formation of Co^{2+} species, which are crucial for hydrogen dissociation and the cleavage of C–O bonds.[48] Furthermore, Pd–Zn bimetallic catalysts with the PdZn alloy were also reported for the conversion of HMF.[45] For the PdZn catalyst, the interaction between Pd and Zn induced electron transfer from Pd to Zn, promoting the activity of Pd species. Thus, the incorporation of Zn enhances the electron-donating capacity of Pd while diminishing its electron-accepting capability. The PdZn(111) plane exhibits stronger oxygen adsorption compared to the Pd(111) plane, which alters the adsorption configuration of HMF and intermediates, producing BHMF in a high yield.[45]

As noble metals, Pt-based bimetallic catalysts have also been studied. Wen *et al.* recently developed a thermodynamically driven method for synthesizing ultrasmall PtCo alloy nanoparticles. Metal precursors are uniformly distributed into nanoscale compartments within a microemulsion, followed by alloying at elevated temperatures. The electron transfer from Co to Pt in PtCo alloys creates Pt sites enriched with electrons and Co sites deficient in electrons, enhancing selectivity towards DMF, which was produced in a yield above 99% under mild conditions of 120 °C and 1 MPa H_2.[57] In addition, the PtCo alloy formed on the support like Al_2O_3[60] and carbon[56] has also been reported. The product selectivity largely depends on the reaction temperature. At 40 °C, the $Co_1Pt_{0.050}Al$ catalyst with larger Pt loading enabled a yield of BHMF exceeding 99.9%, whereas the $Co_1Pt_{0.013}Al$ catalyst produced DMF in a 86.7% yield at 160 °C.[60] Usually, the DMF formation on the Pt_3Co_2/C catalyst largely depends on the reaction temperature, with a yield of 75% at 120 °C, increasing up to 98% at 160 °C.[56]

Moreover, a kind of PtNi/SBA-15 catalyst was synthesized *via* a hydrothermal method, using poly-vinylpyrrolidone as a surfactant to control the formation of PtNi nanoalloys within SBA-15 pore channels. A strong electron transfer existed between Pt and Ni, forming surface $Pt^{\delta-}$–$Ni^{\delta+}$ pairs; in addition, the active hydrogen spilled from Pt to Ni and to the SBA-15 support, thus promoting selective hydrogenation of the C=O bond. BHMF was produced in a yield of 68.2% at 30 °C, 1.5 MPa H_2, for 2 h.[63] A similar electron transfer was also reported on the Pt/Ni@C catalyst, the electron-rich $Pt^{\delta-}$ species favor the adsorption and activation of the C=O bond in HMF

by donating electrons to the carbonyl groups. Thus, BHMF was produced in a yield of 98% at 100 °C, 2 MPa H_2, for 2 h.[64] Moreover, the incorporation of Ir into Pt/CMK[53] results in the formation of electron-deficient Pt on the alloy surface, synergistically enhancing the adsorption and activation of C=O groups in both the substrate and intermediates, thereby improving the selectivity towards DMF.

The Ru-based bimetallic catalyst was seldom studied. For the catalytic conversion of HMF, it is difficult to form the Ru-based metallic alloy,[68,69,71,72] except for one report of Ru-Ir/C catalysts.[67] The electron transfer from Ru to Ir on the RuIr alloy nanoparticle formed electron-sufficient Ir^0 and electron-deficient Ru^0 species on the surface of Ru–Ir/C catalyst, which benefit the adsorption of the C=O group in HMF and MF, thereby markedly accelerating the conversion of HMF to produce DMF with a 99% yield at 120 °C and 1 MPa H_2.

Non-noble metal catalysts have garnered significant attention due to their advantages of low costs compared with the noble metal catalysts in large-scale industrial applications. Cu- and Ni-based catalysts are mostly studied among non-noble bimetallic catalysts, and Co-based bimetallic catalysts have also been reported for the catalytic conversion of HMF. In Cu–Co bimetallic catalysts, Cu and Co typically exist as highly dispersed nanoparticles on the catalyst surface rather than forming CuCo alloys.[75,77] However, an exception is the CuCo/Al_2O_3 catalyst, where a CuCo alloy and a Co@CuCo core–shell structure were formed. The synergistic effect of the local atomic arrangement and electronic structure in the Co@CuCo core–shell significantly improve low-temperature activity, achieving a 91.7% yield of DMF under mild conditions (130 °C, 1 MPa H_2). The CuCo alloy shell helps prevent oxidation of the Co core, preserving its high H_2 dissociation capability. Additionally, the electronic structure of the CuCo alloy facilitates C–O bond cleavage, enhancing the hydrodeoxygenation of HMF.[74] In addition, CoCu alloy has also been reported to be effective for ring-opening hydrogenolysis of HMF; on a kind of Co_xCuAl LDO catalyst, a CoCu alloy with electron-rich Co was formed, which promoted the ring-opening hydrogenolysis to produce 1,2,6-HTO in 72% yield at 120 °C.[111] In this case, the electron-rich Co within the formed CoCu alloy was active for both efficient hydrogenation and ring-opening hydrogenolysis, while due to the lack of this active site in monometallic catalysts, only the hydrogenated product (BHMF) was achieved with CoAl or CuAl. The adsorption experiments and DFT calculations revealed that the bimetallic catalyst exhibited a superior activity for HMF and H adsorption compared to the monometallic catalysts, owing to the formation of the CoCu alloy, which resulted in a higher d-band center attributed to the electron-rich Co.[111]

While, CuNi alloy is easy to form compared to CuCo. For example, a kind of NiCu/C catalyst containing NiCu alloy and Ni_1Cu_3 nanocrystals having a Ni : Cu molar ratio of 1 : 1 with a Cu-rich core and a shell was also reported.[85] The formation of the core–shell structure is due to the case of Ni oxidation during preparation, leading to Ni segregation on the particle surface. For HMF conversion, the monometallic catalyst with

active Ni^0 species on the surface promotes C=C bond hydrogenation, leading to the formation of DMTHF, while Cu^0 enhances hydrogenolysis, resulting in the formation of DMF. On the bimetallic catalysts, the presence of NiCu alloy active sites allows for a balance in production of DMF and DMTHF.[85] In addition, a NiZn alloy catalyst was synthesized through controllable reduction of a mixed oxide derived from NiZnAl hydrotalcite. Zn modified the electronic structure of Ni atoms, forming electron-rich Ni, which favors for C=O bond activation. The isolated electron-rich Ni species preferentially promotes the cleavage of the C–O bond, leading to a 93.6% high selectivity of DMF.[100] Furthermore, it was reported that a mixed metal oxide catalyst of NiCoAl showed a 64.5% yield of 1,2,6-HTO under the mild reaction conditions of 120 °C and 4 MPa H_2. The cooperation between the Co and Ni species provides a synergetic effect to catalyze the ring opening of the furan ring. However, this cooperation requires a proper interaction between the Ni and Co active sites and an appropriate ratio of Ni/Co to balance the C–O cleavage and subsequent hydrogenation. CoO is mainly responsible for the adsorption of the furan ring and C–O bond cleavage, while the Ni site catalyzes hydrogenation.[108] The change of the crystallographic phase affecting the adsorption configuration was reported on the $Ni_{1.5}GaAl$-LDO catalyst by Nie et al.[98] They prepared a series of hydrotalcite-derived NiAl-LDO and NiGaAl-LDO catalysts and found that the BHMTHF was produced in a high yield of 99% on the NiAl-LDO catalyst. However, BHMF was produced with a yield of 95.6% on the $Ni_{1.5}GaAl$-LDO catalyst. It was certified that Ga doping can induce a charge transfer to disrupt Ni arrangement, forming an electron-rich Ni_3Ga alloy; this weakens the adsorption of the furan ring and prohibits ring hydrogenation, resulting in the production of BHMF.[98]

Intermetallic compounds and others. In addition to the formation of alloy phases as mentioned above, bimetallic catalysts can also give rise to intermetallic compounds. An intermetallic compound is a kind of compound with an ordered structure and fixed composition, where the metal atoms are bonded through a metallic, ionic, or covalent bond. The formation of an intermetallic compound changes the electronic structure of metals by rearranging electrons between different metal atoms to form an ordered intermetallic structure. Thus, the intermetallic compound formed in the bimetallic catalyst will affect the adsorption mode of HMF, affecting the product distribution. It was reported that Pt_3Sn_1 formed on the bimetallic catalyst of PtSn/g-C_3N_4 by precisely controlling the atomic ratio of Pt/Sn in the preparation (deposition–precipitation). There is an electron transfer from Sn to Pt, forming electron-rich $Pt^{\delta-}$ species, which favor the adsorption of the C=O bond in HMF, as illustrated in Fig. 4. Thus, the PtSn/g-C_3N_4 catalyst with Pt_3Sn_1 (Pt/Sn = 3) gave a high yield of BHMF (>98%) under mild conditions of 80 °C and 2 MPa H_2. Nevertheless, when the ratio of Pt/Sn decreases with raising Sn loading, the adsorption of C=O becomes weaker, resulting in a sharp decline of activity. As a result, conversion of HMF drops to 38% from 100%, and the selectivity of BHMF decreases slightly from 98.1% to 92%.[54]
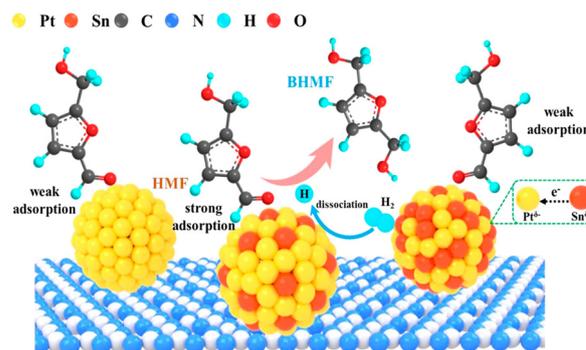

Fig. 4 Corresponding reaction mechanism diagram of Pt_3Sn_1/g-C_3N_4. Reproduced from ref. 54 with permission of American Chemical Society, Copyright 2024.

Zhang et al. synthesized Ni–Ga intermetallic compounds at varying Ni/Ga ratios via a hydrothermal approach. The Ni_3Ga_1 intermetallic and reference Ni catalysts were prepared by adjusting the type and quantity of metal precursors using an identical method. Among several non-precious metals that can form intermetallic compounds with Ni, Ga was selected for its superior adjustability in the ratio of Ni/Ga, allowing precise control over the composition. The incorporation of Ga results in electron transfer from Ga to Ni, disrupting the contiguous array of Ni sites that are susceptible to adsorbing the furan ring. This disruption effectively reduces side reactions and enhances the selectivity and yield of BHMF (98.4%) in the aqueous phase at 3 MPa H_2 and 120 °C. The Ni–Ga intermetallic catalysts with Ni_1Ga_1 (110) or Ni_3Ga_1 (111) as the most exposed facet were reported. Kinetic investigations unveiled a reaction order trend for HMF hydrogenation in a sequence of $Ni_1Ga_1 > Ni_3Ga_1 > Ni$ catalyst. Notably, the reference Ni catalyst exhibited a negative reaction order, indicating an inhibitory effect stemming from HMF-induced site blocking. In contrast, the Ni–Ga intermetallic compound demonstrated a positive reaction order, implying that the pronounced adsorption of HMF on the pure Ni surface could be mitigated over the Ni_1Ga_1 (110) and Ni_3Ga_1 (111) facets.[99]

Moreover, Gross's team has developed a simple method for synthesizing Pt–Co bimetallic nanoporous networks (BNNs). Their study reveals that a kind of intermetallic compound of Pt_3Co was formed on the surface of the catalyst at a reduction temperature of 170 °C, which favor the cleavage of the C–O bond and exhibit a higher selectivity of 78% towards DMF. However, when the catalyst was reduced at 300 °C, the intermetallic compound of Pt_3Co was transformed to the separated nanoparticles of Pt and CoOx; in such a case, the C–O cleavage was significantly prohibited. On the PtCo (BNN) catalyst composed of segregated Pt and Co domains formed at an elevated reduction temperature of 300 °C, the two main products of 2,5-bis(hydroxymethyl)furan and MF were produced.[59]

Electronic effects also exist in adjacent metal–metal nanoparticles and metal–metal oxide particles in bimetallic catalysts. The electronic interaction between metal–metal particles

can be modulated by tuning the metal ratio and structure, thereby optimizing reaction pathways and improving the selectivity of target products. Zhang *et al.* prepared a series of PdAu$_x$/GC800 catalysts by varying the Au/Pd mass ratio. The intimate contact and strong interactions between Pd and Au nanoparticles lead to charge transfer from Au to Pd, forming larger amounts of active Pd^0 species and highly dispersed smaller Pd and Au particles. The PdAu$_4$/GC800 exhibited a high selectivity of 94.4% towards DMF with 86.8% HMF conversion at 150 °C.[40] Similarly, Pt and Co dispersed on multi-walled carbon nanotubes (MWCNTs) have been reported. The electronic transfer from Co^0 to Pt^0 results in a positive charge density on Co atoms and a negative charge density on Pt atoms, facilitating the adsorption of C–O over a Pt$^{\delta-}$–Co$^{\delta+}$ site and decreasing the probability of adsorption *via* the furan group. Thus, the synergistic effect between Pt–Co and MWCNTs is crucial. The DMF yield reached 92.0% in *n*-butanol at 160 °C.[58] The electron transfer from Co to Pt was also found on the PtCo/LOC (PtCo clusters on La$_2$O$_2$CO$_3$) bimetallic catalyst with Pt atoms covered by Co species for ring-opening of HMF into 1,2,6-HTO in water. The increased electron density of Pt species is deemed highly beneficial for activating H$_2$ and reducing the strength of Pt–H bonds, further increasing the [H*] coverage at metal sites, which refutes the reduction of the local fraction of [H*] driven by electronic modification. Bimetallic nanoclusters would provide fewer [H*] species than bare Pt metal surface. The 1,2,6-HTO yield of 79.8% was obtained over the PtCo/LOC catalyst under the mild conditions of 120 °C and 1 MPa H$_2$.[37] The positive effects of doping Co on the catalytic performance of the PtCo bimetallic catalyst to yield 1,2,6-HTO were also reported on PtCo/CeO$_2$.[36,62]

Compared with mono-metal catalysts, the bimetallic catalysts with an alloy or intermetallic compound formed on their surface often showed high catalytic stability. The deactivation of the catalyst in HMF conversion is mostly caused by coking, which typically results from side reactions like over-hydrogenation and condensation,[56] which can be effectively mitigated by the unique electronic and geometric properties of the bimetallic alloy catalytic system. On the other hand, the formation of bimetallic alloy can promote the dispersion of metal species and inhibit metal agglomeration.[51,53] Thus, the bimetallic alloy catalysts are more tolerant against sintering[33,51] and water resistance.[63]

Geometric structure

Doping a second metal induces geometric restructuring of the primary metal nanoparticles through strong metal–support interactions (SMSI) in bimetallic catalysts. This restructuring can manifest in the following ways: (1) forming atomic isolation by the doped metal, leading to highly dispersed active sites, preventing the aggregation; (2) forming encapsulated or core–shell structures *via* doped metal oxides or carbon overlayers, preventing oxidation or leaching of the active sites. (3) Oxygen vacancies are particularly important for C=O and C–O bond activation of HMF. The synergy between bimetallic

species and oxygen vacancies at the metal–support interface can boost the catalytic performance.

Encapsulation. Encapsulation is one of the core manifestations of SMSI, referring to the migration and coverage of a metal oxide or carbon material on the surface of primary active metal particles under the thermal treatments with air and/or H$_2$. Thus, the leaching and aggregation of active metal species will be prohibited, enhancing the stability. Schüth *et al.* developed a method for the synthesis of a kind of PtCo/HCS catalyst with encapsulated PtCo bimetallic particles in the hollow carbon sphere (HCS) by a hydrothermal process combined with ion exchange and pyrolysis processes with a soft-templating method using EO$_{20}$-PO$_{70}$-EO$_{20}$ (P123) and sodium oleate (SO) as double surfactants. It involves three key steps: (1) preparation of hollow polymeric spheres (HPS) by forming mixed micelles by a hydrothermal method using double surfactants of P123 and SO; the diameters and shell thicknesses are controlled *via* polymerization of 2,4-dihydroxybenzoic acid and formaldehyde at the surface of emulsion droplets mediated by weak acid–base interactions. (2) Introduction of platinum salt into the above P123/SO system. Platinum species adsorbs onto the emulsion droplet surfaces through interactions with the PEO segment of P123 and the carboxylate group of SO. Then the platinum salt is reduced to Pt nanoparticles by formaldehyde during hydrothermal treatment and encapsulated within the HPS, forming Pt@HPS. (3) Cobalt salt was introduced into the formed Pt@HPS with abundant carboxylate groups on its surface to bind Co^{2+} species, leading Co to deposit onto the surface of Pt metals located in the hollow cores during the pyrolysis step, resulting in the formation of bimetallic nanoparticles (PtCo@HCS) under a H$_2$/Ar atmosphere at 500 °C. The encapsulated bimetallic catalysts such as Cu$_3$Pd@HCS, CoPd$_2$@HCS and Cu$_3$Pt@HCS were also prepared using the same methodology. These materials have structures and morphologies similar to the PtCo@HCS with metallic nanoparticles encapsulated in the hollow carbon sphere. The PtCo@HCS catalyst exhibited high efficiency for selective conversion of HMF, producing DMF with a yield above 98% at 180 °C, 1.0 MPa H$_2$.[61] Besides, Gorte *et al.* developed a Pt$_3$Co$_2$ catalyst consisting a Pt-rich core and a CoOx surface monolayer. DFT calculations reveal that the CoOx monolayer interacts weakly with the furan ring of HMF to prevent side reactions, including over-hydrogenation and ring opening, while boost the hydrodeoxygenation of C–O bond cleavage, producing the desired product of DMF with a high yield of 98%. The Pt$_3$Co$_2$ is more selective than Pt$_3$Co$_1$ due to the difference in particle surface structure. Pt$_3$Co$_1$ does not have enough Co atoms to completely cover the surface, leading to the presence of uncovered Pt sites and therefore causing side reactions. Moreover, in contrast to the monometallic catalyst, Pt$_3$Co$_2$ presented higher stability with almost no morphological changes after long term use. The particle aggregation was prohibited by the special structure of the active Pt$_3$Co$_2$ core, which is covered by a CoOx monolayer.[56] Feng and Li *et al.* prepared a core–shell structured Co@CuCo catalyst with a CuCo alloy shell coated on the Co core by high temperature

reduction of layered double hydroxides (LDH) of CuCoAl-LDHs at >700 °C.[74] The formation of the core–shell structure is ascribed to the difference in the migration and reduction rates of Cu and Co species during the reduction due to their different surface free energies (Cu, 1.934 J m^{-2}; Co, 2.709 J m^{-2}).[114,115] Cu^{2+} is firstly reduced to metallic Cu nanoparticles, after which CoOx begins to reduce gradually. As the reduction temperature increases, the reduction degree increases, and atomic rearrangement intensifies. Cu gradually accumulates on the surface, forming a CuCo alloy layer, while Co gradually concentrates in the core of the nanoparticles. The CuCo alloy shell can prevent the oxidation of Co components in the core, maintain its high H$_2$ dissociation capacity, and improve the low temperature hydrogenation efficiency. Moreover, the electronic structural changes of the CuCo alloy shell can jointly promote the hydrodeoxygenation reaction of the C–O bond. Thus, the Co@CuCo catalyst achieved a decent DMF yield of 91.7% under mild reaction conditions of 130 °C and 1 MPa H$_2$.[74]

Chen et al. reported a Cu–Co@C catalyst with bimetallic nanoparticles entrapped by carbon shells, which was prepared by a modified Pechini-type sol–gel method and heated at 800 °C under argon flow for 2 h. The Cu–Co@C catalyst can produce DMF in a high yield of 99.4%, and presents good stability without loss in activity after being recycled 8 times. It is much more stable than the Co@C catalyst. The doped Cu and surface coated carbon shell protect the active Co species from oxidation and deactivation during the reaction.[77] The encapsulation of bimetallic active species with a carbon layer promotes the catalytic performance, especially the catalytic stability in the conversion of HMF; similar results were also reported on PtNi@C,[64] Fe–Ni/NPCM[97] and CoNi@NC.[107]

Metal–N(S) species – new active sites. The strong metal–support interaction can create a new active species by coordination of primary metallic species with an element of support. The most studied catalyst support is nitrogen doped carbon materials, due to the strong bonding and coordinating ability of nitrogen. Gui et al. developed a series of Pd immobilized Co-CoOx@ N-doped C catalysts from the pyrolysis of the ZIF-67 support. They demonstrated that both Pd and Co interacted with nitrogen and formed Pt–N and Co–N species on the surface of the catalyst by XPS and TEM. The surface Pd NPs were anchored on the ZIF-67-derived support through surface N atoms, and these N atoms should be adjacent to the formed CoOx due to strong Co–N interactions. Pd NPs having intense interactions with CoOx made the dissociation of H$_2$ into active hydrogen species easier. Subsequently, the as-formed active hydrogen spilled quickly to the adjacent CoOx surface. Their interaction, in turn, promoted the hydrogenation of the HMF carbonyl group to form hydroxymethyl groups. Then, fast hydrogenolysis occurred to produce the target product DMF in high yield of 97.8% at 180 °C and 1.5 MPa H$_2$. Importantly, the catalyst also exhibited high stability under the reaction conditions benefited from the protection of the surface NC layers.[49]

Moreover, Chen et al. synthesized a nitrogen-doped carbon supported CoMo bimetallic catalyst (CoMo@NC) through the pyrolysis of CoMo-doped ZIFs. This catalyst, featuring CoN$_4$ single-atom sites and a low Co content (0.14 wt%), demonstrated superior catalytic activity. The strong metal–support interactions in CoMo@NC facilitate coordination between the metals and the support, leading to the formation of MoC species and CoN$_4$ single-atom sites. DFT calculations revealed that HMF primarily adsorbs on the Mo species, while H$_2$ adsorption and activation occur predominantly on the Co sites. The CoMo@NC catalyst achieved an impressive 97% yield of DMF at 170 °C and 1.5 MPa H$_2$.[110] Similarly, the CuCo@NC catalyst was also prepared by using the same method, and Co interacted with nitrogen forming a new Co–Nx species. The CuCo@NC catalyst gave a 92.4% selectivity towards BHMF at 100 °C and 1 MPa H$_2$.[78] Besides, on the PdCo$_8$/S-CNT catalyst, Co coordinates with sulfur to form Co$_9$S$_8$ species, which were dispersed with Pd nanoparticles separately on the surface of the catalyst. The synergistic effect of Pd and Co$_9$S$_8$ double active sites endows the catalyst with high catalytic performance; Pd mainly catalyzes the hydrogenation of C=O bonds and Co$_9$S$_8$ plays a role in catalyzing C–O bond hydrogenolysis.[50]

Oxygen vacancies. Oxygen vacancies (Ov), a kind of main defect, which are easily formed on reducible or oxophilic metal oxides such as TiO$_2$, CeO$_2$, WO$_3$, and ZrO$_2$, play a crucial role in the heterogeneous surface catalysis. Oxygen vacancies serve as active sites for the adsorption and activation of reactants, especially the oxygen containing functional group. The number of oxygen vacancies can be significantly enriched by incorporating external elements with variable valence onto the reducible support. The presence of vacancies can reduce the energy barrier of C–O bonds via intense interaction and adsorption.[116,117]

The construction of surface Ov can not only facilitate the adsorption of the carbonyl group in the molecule HMF but also enhance the electron transfer, improving the performance of the catalysts. For example, Cui and Liu et al. synthesized a series of Pd immobilized Co-CoOx@N-doped carbon catalysts from pyrolysis of the ZIF-67 material, on which abundant surface defects formed during pyrolysis at temperatures above 700 °C. It showed high catalytic activity, selectivity, and stability in the conversion of HMF with high selectivity of DMF (97.8%). They proposed a catalytic mechanism as shown in Fig. 5. The mesoporous N-doped carbon itself, as a Lewis base, facilitates the effective adsorption of the HMF molecule and the intermediates through the O–H⋯N interaction. The Co^{2+} species adjoining the Ov on the support can fix the oxygen atom of the C=O bond in HMF by electronic interactions, thus leading to the formation of Co^{3+} species and the reduction of the C=O bond. The oxygen of the aldehyde group in HMF then takes up Ov adjoining Co^{2+}. The interaction of HMF with the Co^{2+}–Ov–Co^{2+} defect structure could remarkably motivate the chemical adsorption of HMF to facilitate the hydrogenation of the C=O bond. Therefore, the superior electron transfer nature of this material benefits the cascade reaction from HMF to DMF.[49]

Similarly, the Ov promoting C–O bond cleavage in the conversion of HMF was also reported on a bimetallic PdCo/Mo$_2$C catalyst.[48] The authors found that addition of Co increases the
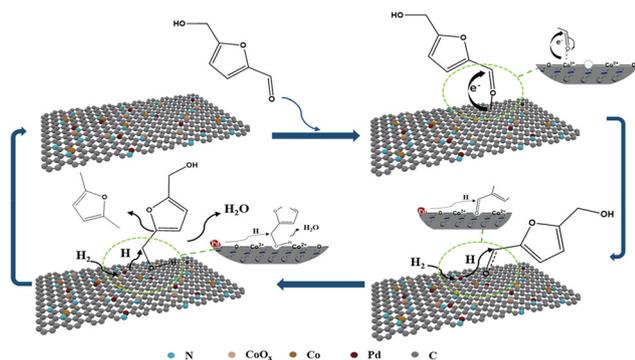
Fig. 5 Possible reaction mechanism of the Pd/Co-CoOx@CN for HMF hydrogenolysis into DMF. Reproduced from ref. 49 with permission from American Chemical Society, copyright (2020).

content of the β-Mo$_2$C phase, and MoCx provides more Ov compared to MoO$_3$. The bimetallic PdCo species promotes hydrogen dissociation and the Ov facilitates the cleavage of the C–O bond. The synergistic effects of PdCo and Ov endow the catalyst with high catalytic performance in the conversion of HMF. A similar function of Ov was also reported on the RuCo/Co$_3$O$_4$ bimetallic catalyst.[70]

Moreover, Wang *et al.* designed a CuCo/CeOx catalyst with a number of Ov generated by the introduction of Co species into the CeOx lattice. DFT calculations confirmed that the Ov and the CoCe–Ov interface contribute to the activation of C═O and C–O bonds and prohibition of the ring opening reaction. For the Cu–Co/CeOx catalyst, Cu species was the main active site for hydrogen dissociation; the Ov and CoCe–Ov interface promote the C–O cleavage of the hydrogenolysis of MFA, which is the key step of HMF converting into DMF. Thus, the synergistic effects of Cu, CoOx, CeOx and Ov enhance the catalytic performance of Cu–Co/CeOx catalysts to achieve a high DMF yield of 96.5%.[76]

Acidity

Introducing a second metal can change the acidity of a metal supported catalyst due to the electronic interactions between the metals and the metal–support interface. By rationally adjusting surface acid properties, catalytic activity and selectivity can be improved or fine-tuned. The surface acidity of bimetallic catalysts primarily originates from two sources: (1) the metal oxide formed by a second metal, where the metal oxide acts as a Lewis acid site. (2) The acidic support or synergistic interaction between the metal and the support. In the catalytic conversion of HMF, surface acidity significantly influences the reaction pathway and product selectivity. As is known, the suitable acidity facilitates the C–O cleavage and favors hydrogen transfer on the surface of the catalyst, while the high acidity promotes the C–C cleavage and the furan ring opening reaction. Thus, the surface acidity is crucial for producing the desired furan or tetrahydrofuran products in HMF conversion.

New acid sites from the doped metal. When a second metal is doped, an extra metal oxide will be formed and anchored on the metal supported catalyst. These metal oxides act as acid sites to enhance the surface acidity of the catalyst, such as ZnO, NiO, FeOx, MnOx, MoOx, CoOx, *etc.* For instance, Zhong *et al.* prepared a kind of zinc-modified cobalt dispersed on a nitrogen–carbon support of the ZnCo/N–C catalyst. ZnO nanoparticles were formed and highly dispersed on the surface of the catalyst, increasing the surface acidity largely. They demonstrated the synergistic effects of the ZnO acid site and Co particles endowed the ZnCo/N–C catalyst (Zn/Co = 1:3) with superior performance in the selective conversion of HMF, producing DMF in a high yield of 93.5%. The comprehensive characterization revealed that the Co active site activates H$_2$ to produce H atoms, the ZnO acidic site activates the hydroxyl/carbonyl group, which synergistically enhances the selective hydrogenolysis of HMF to DMF *via* the key intermediates of BHMF and MF.[112] The similar synergistic effect of the NiO acid site was also found in Cu–Ni/BC[86] and Ni$_{0.74}$Fe$_{0.97}$Al;[96] these catalysts exhibited high performance in selective conversion of HMF into DMF.

The doping of oxophilic metals like Fe,[65,66,95,109] Mn[104] and Mo[71] can easily form metal oxides and increase the acidity of the catalysts, enhancing the hydrogenolysis process. Ma *et al.*[65] have studied the effects of doping Ni, Co, Fe and Mo on the acidity and catalytic performance of active carbon supported Pt-based (PtM/C) catalysts. All the catalysts studied present both the Brønsted and Lewis acid sites. It was reported that Lewis acid sites can facilitate the breakage of C–O bonds, leading to the hydrogenolysis reaction; Brønsted acid sites promote the activation of the carbonyl group, favoring the preferential hydrogenation of the C═O bond.[118] Among the studied catalysts, the PtFe/C catalyst containing moderate acidity with balanced Brønsted and Lewis acid sites demonstrated a good balance between hydrogenation and deoxygenation activity, yielding 99.6% of DMF. The high catalytic performance was attributed to the synergistic interactions between Pt and FeOx species, while the PtNi/C catalyst possessing more Brønsted acid sites and an appropriate amount of Lewis acid sites demonstrated high hydrogenation activity, particularly for furan ring hydrogenation to form a byproduct of DMTHF through further hydrogenation of DMF.[65] A similar synergistic interaction between Pt and FeOx species was also reported in PtFe/AC by Liu *et al.*[66] It was reported that incorporation of Fe into the Co-based catalyst of Co–FeOx/NC could enhance the surface acidity.[109] The surface of the catalyst contains abundant Co and FeOx interfaces; the interfacial Co presents an electron-deficient state caused by electron transfer from Co to FeOx, improving the hydrogen activation and subsequent spillover to interfacial FeOx, and the interfacial FeOx derives abundant acid sites, facilitating the adsorption and activation of HMF. Under the cooperation of interfacial Co and FeOx, the hydrogenolysis of HMF was significantly improved to produce DMF with a high yield of 99.9%. A catalytic mechanism was proposed, as shown in Fig. 6. H$_2$ initially undergoes dissociation to active H species at the Co sites, and then H migrates to the FeOx acid sites *via* hydrogen spillover. The HMF molecules adsorb on the FeOx acid sites with its C═O
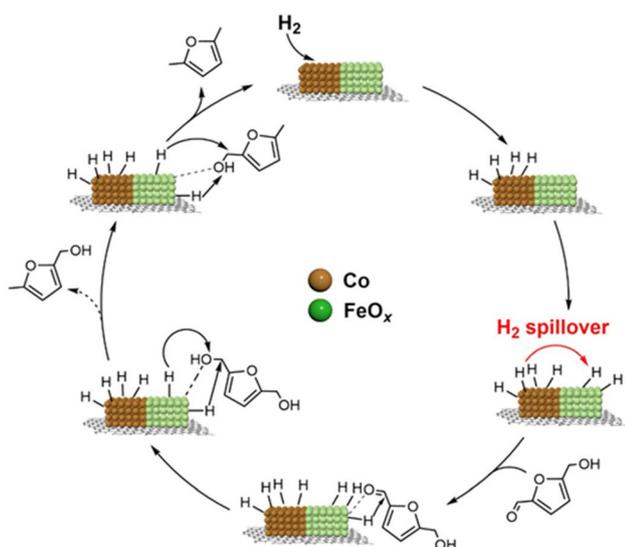
Fig. 6 Plausible reaction mechanism for the hydrodeoxygenation of HMF to DMF over Co–FeOx interfaces. Reproduced from ref. 109 with permission from ELSEVIER, copyright (2024).

bond hydrogenating to BHMF, and then the C–O bond cleaves to MFA; finally, the other C–O bond breaks to produce DMF.[109]

Moreover, Mn as a second metal doped to the Ni/AC catalyst can form a MnOx phase on the surface of the Ni–Mn/AC catalyst; the doped Mn promotes the reduction of Ni species and increases the surface acidity by forming MnOx. The synergistic effect of MnOx Lewis acid sites with the highly dispersed Ni^0 species results in a 98.5% yield of DMF under the reaction conditions of 180 °C and 2.0 MPa H_2 for 4 h.[104] In addition, CoOx was also reported to form acid sites on the surface of the bimetallic Ru–Co/AC catalyst, which are responsible for activating and cracking the C–O bonds in HMF. Ru NPs act as the active sites for hydrogenation. As a result, DMF was produced in a high yield of 97.9% due to the synergistic effect of Ru^0 and CoOx species.[68] Besides, similar functions of metal oxide were also reported in Mo doped catalysts such as Ru-MoOx/C.[71]

On the other hand, when a Lewis acid of $ZnCl_2$ was combined with the Pd/C catalyst together to catalyze the selective conversion of HMF, DMF was produced in a yield of 85% in the $ZnCl_2$-Pd/C catalysis system, and a similar catalytic performance was also achieved on the bimetallic catalyst of Pd/Zn/C under similar reaction conditions. Control experiments revealed that $ZnCl_2$ is inactive, while Pd/C alone produces significantly less DMF, suggesting that the doped Zn species on the Pd/Zn/C bimetallic catalyst acts as acid sites similar to $ZnCl_2$, promoting the C–O bond cleavage.[46]

Bifunctional catalysts with metal-acid active sites are effective for producing DMF, while the acid intensity is also an important factor in controlling product selectivity, not the stronger, the better. For example, the acidity of the Cu/Al_2O_3 catalyst reduced after doping with Ag species and the number of weak to strong acid sites changed. The $Cu–Ag/Al_2O_3$ catalyst with balanced distribution of weak and strong acid sites and

high Cu dispersion produced DMF in a yield of 93% at 180 °C and 1.5 MPa H_2, which is much higher than that obtained over the Cu/Al_2O_3 catalyst.[73] Similar results were also reported on a potassium doped K–Cu/Al_2O_3 catalyst, on which BHMF was produced in 98.9% yield at 120 °C and 2 MPa H_2.[82] Moreover, it was also reported that the surface acidity can be adjusted by doping a minor amount of Pt into the Co/Al_2O_3 catalyst. The catalytic performance varied with Pt loading; for the $Co_1Pt_{0.050}Al$ catalyst with high Pt loading, strong acidity was observed, achieving a high BHMF yield of >99.9% at 40 °C. In contrast, the $Co_1Pt_{0.013}Al$ catalyst with low Pt loading showed weak acidity, giving a high DMF yield of 86.7% at 160 °C. On these catalysts, Pt^0 and CoOx accompanied by a minor amount of PtO_2 and Co^0 species coexist and these species act as the active sites for hydrogenation and hydrogenolysis in the conversion of HMF.[60]

The surface acidity modified/generated by synergistic effects. For the heterogeneous catalyst, acid support, such as Al_2O_3, ZrO_2, CeO_2, zeolites of HY, ZSM-5 and others, is usually selected for fabricating the metal–acid bi-functional catalysts. As described above, the selective conversion of HMF into DMF requires acid sites with moderate intensity to promote C–O bond cleavage. The doping of a second metal in the bimetallic catalyst can modulate the surface acidity through interaction with the support by changing acidity or creating new acid sites with the doped metal species. Generally, the primary metal in the bimetallic catalysts is responsible for the dissociation of hydrogen and the hydrogenation of the C=O bond, and the synergy of the doped second metal with the support facilitates the cleavage of the C–O bond. The natural acidity of the support largely affects the catalytic performance; for example, Sanjay Srivastava *et al.* have studied the metal–support interaction and the surface acidity of Cu–Co bimetallic catalysts supported on CeO_2, ZrO_2 and Al_2O_3 supports. They demonstrated that the interactions of Cu and Co with the support depend on the nature of the support used, which determines the textural properties, electronic state, and composition of Co and Cu. The relatively weak interaction of Al_2O_3 with Co and Cu induced higher reducibility of Cu–Co/Al_2O_3 compared to Cu–Co supported on ZrO_2 and CeO_2, and the highly dispersed Cu–Co particles on the Al_2O_3 support. In addition, the total amount of acid is in the order of Cu–Co/Al_2O_3 > Cu–Co/ZrO_2 > Cu–Co/CeO_2. Cu–Co/Al_2O_3 showed high catalytic activity and selectivity towards DMF, achieving a 78% yield of DMF, which was attributed to the synergy between surface metallic Cu sites and partially reduced CoOx sites, as well as the appropriate weak/strong acid sites. While, Cu–Co/ZrO_2 showed similar activity but lower selectivity towards DMF due to the differences of Cu–Co metallic states and more strong acidic sites on its surface.[75] Similar results of the surface acid intensity affecting the activity and selectivity were also reported on bimetallic catalysts of NiCoTi-8. The NiCoTi-8 catalyst (molar ratio of Ni : Co : Ti at 4 : 4 : 1) contains both weak and strong acid sites, showing higher activity (90.7% conversion of HMF) and selectivity towards DMF (95.8%). However, the NiCoTi-4 catalyst (molar ratio of Ni : Co : Ti at 2 : 2 : 1) containing much

more strong acid but no weak acid shows very low activity (20.3% conversion of HMF) and a slight decrease in selectivity of DMF (90.0%).[105]

On the other hand, Pisal et al.[47] studied a series of Pd-based bimetallic catalysts of M (M = Ni, Co, Cu, and Pd) supported on Al–Zr mixed oxide (AZMO$_{CP}$) catalysts prepared by combining co-precipitation, hydrothermal and impregnation methods. The characterization and experimental results demonstrate that the 2%Pd5%Co/AZMO$_{CP}$ catalyst with a higher surface area and acidity presented high efficiency for hydrogenation of HMF, giving DMF in 97% yield at 100 °C and 1.0 MPa H$_2$. They proposed that HMF was adsorbed on the acidic site, and hydrogen was adsorbed and dissociated on the metallic site.[47]

Moreover, the synergistic effect of acid and base sites on catalytic performance were also reported.[101] Yang et al. studied a kind of Ni$_2$In/MgO-Al$_2$O$_3$ catalyst with both the surface acid and base sites. They demonstrated that the inactive atoms geometrically isolate the active sites and modulate the electronic structure of Ni and the surface acid–base microenvironment. The synergistic catalysis between metal active sites and the acid–base sites favors the C=O hydrogenation and C–O hydrogenolysis, promoting the cleavage of the C–O bond, thus producing DMF in high yield of 93.2%. They proposed a catalytic mechanism for HMF hydrogenation to DMF on the Ni$_2$In/MgO–Al$_2$O$_3$ catalyst, as shown in Fig. 7. Initially, the HMF molecule is adsorbed on the surface of Ni$_2$In through adsorption of C–O and hydrogenates to BHMF. Subsequently, the C–O group in BHMF is adsorbed on the surface of Ni$_2$In. Meanwhile, the acid and base sites serve as auxiliary active sites to accelerate the C–O bond breakage. The adsorbed BHMF undergoes hydrogenolysis to MFA and then hydrogenolysis to the final product DMF via synergistic catalysis of Ni$_2$In and acid–base sites.[101]

In addition, introducing a second metal can modify the alkalinity of the catalyst, thus improving the cleavage of the C–O bond in the furan ring to promote the ring-opening reaction. Shao et al. prepared a kind of CuMgAl catalyst from LDH for the hydrogenation of HMF to produce 1,2-HDO. Incorporating Mg species into the CuAl induced the formation of abundant

medium strength basic sites on the surface of the catalyst, weakening the interaction between Cu species and the support. The basic sites in CuMgAl facilitate the adsorption of C=O and C–O–C bonds, promoting the subsequent ring opening of MFA (reaction intermediate) through hydrogenation/hydrogenolysis over Cu active species, producing 1,2-HDO in a yield of 42% at 150 °C and 6.0 MPa H$_2$. Furthermore, the MgAl LDH structure used as the precursor of CuMgAl catalysts improved the stability of catalysts via suppressing the sintering of Cu nanoparticles, which maintained superior reusability over catalysts as the polymerization of HMF, the main reason for lowering the selectivity of 1,2-HDO, was prohibited.[21]

Summary and perspectives

The catalytic conversion of HMF primarily proceeds via two ways to produce furan derivatives. One way is hydrogenation of the C=O bond in HMF to form BHMF. Subsequently, the C–OH group undergoes hydrogenolysis to yield MFA, or the furan ring is hydrogenated to produce BHMTHF. Another way is hydrogenolysis of the C–OH group to form MF, followed by C=O hydrogenation to produce MFA; finally, its remaining C–OH group hydrogenolysis yields DMF and the furan ring further undergoes hydrogenation to form DMTHF. Besides, in some cases, the ring-opening hydrogenolysis occurs to produce 1,2,6-HTO or 1,2-HDO in the catalytic conversion of HMF, even though it is difficult to achieve high yield. The polyol formation proceeds with a series of reactions through intermediates BHMF and BHMTHF. Therefore, for the conversion of HMF, an effective catalyst should possess the following advantages: (1) highly dispersed small metallic active sites, which are essential for H$_2$ activation and dissociation; (2) optimal surface acid sites that are necessary to facilitate hydrogen transfer and promote hydrogenation and the C–O bond activation; (3) controlled oxygen vacancies, which are important in strengthen adsorption of C=O and C–O bonds, thereby promote C–O bond cleavage and C=O bond hydrogenation. Thus, bimetallic catalysts are particularly advantageous as they combine these features, as described above.

Bimetallic catalysts have garnered significant attention for their superior catalytic efficiency, selectivity, and stability compared to monometallic catalysts. The incorporation of a second metal or metal oxide induces electronic, geometric, and synergistic effects that modulate the catalytic behavior. These modifications significantly improve metal dispersibility, inhibit metal aggregation, leaching and carbon deposition, and thus enhance catalytic stability.

In bimetallic catalysts, H$_2$ dissociation typically occurs preferentially on the primary metal (e.g., Pd, Pt, Ru, Ni, Cu, or Co), while the adsorption and activation of C=O and C–O bonds often take place at new active sites formed by the doped metal (e.g., Au, Ru, Cu, Co, Ni, Fe, Sn, Ga, Re, Mo or Mn). The catalytic properties of bimetallic catalysts are benefited from (1) the formation of new active sites via bimetallic alloys or
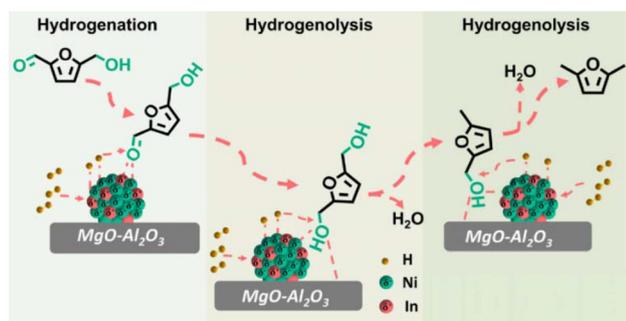

Fig. 7 A proposed hydrogenation–hydrogenolysis mechanism for HMF transformation to DMF over Ni$_2$In/MgO-Al$_2$O$_3$. Reproduced from ref. 101 with permission from ELSEVIER, copyright (2022).

intermetallic compounds, which modulate the electronic structure of the primary metal; (2) core–shell structures, where primary metal particles are encapsulated by the metal oxide shell or carbon materials, forming new metallic species and oxygen vacancies; and (3) modulation of surface acidity (creation of new acid sites or adjustment of support acidity). These structural and electronic modifications enhance catalytic activity, product selectivity and catalyst stability.

Electronic effects

The incorporation of a secondary metal facilitates the formation of alloys or intermetallic compounds, altering the electronic structure of the primary metal and improving metal dispersion. This adjustment in charge density promotes H_2 activation and dissociation while optimizing the adsorption configuration of HMF, thereby enhancing both activity and selectivity.

Geometric structure

Strong interactions between the primary and secondary metals can lead to core–shell structures, where primary metal particles are coated with a metal oxide shell or encapsulated within carbon hollow spheres. Such configurations prevent particle agglomeration and oxidation under harsh reaction conditions, thereby improving catalyst stability. Additionally, oxygen vacancies on the reducible support (e.g., TiO_2, CeO_2, WO_3, and ZrO_2) play a pivotal role in HMF hydrodeoxygenation. These vacancies provide active sites for reactant adsorption and activation, lowering energy barriers and enhancing substrate interaction. In HMF hydrogenation, oxygen vacancies are particularly important for $C=O$ and $C-O$ bond activation. The synergy between bimetallic species and oxygen vacancies at the metal–support interface can boost the catalytic performance.

Role of acidity

Acid sites are crucial for breaking the C–O bond to produce DMF, but excessive acidity will promote the undesired side reactions of furan ring hydrogenation or ring opening, reducing DMF selectivity. Therefore, introducing a second metal to fine-tune acidity and balance weak and strong acid sites is essential. Acid sites can facilitate active hydrogen transfer, accelerating hydrogenation steps. Therefore, precise control of acid strength is crucial for achieving high efficiency in the selective conversion of HMF to a certain desired furan-ring product. In addition, introducing a second metal can modify the alkalinity of the catalyst, improving the cleavage of the C–O bond in the furan ring, resulting in ring-opening reactions.

Challenges and future perspectives

Despite achieving significant progress in bimetallic catalysts for HMF conversion, challenges still remain for large-scale industrial applications: (1) development of non-noble bimetallic catalysts with high performance comparable to noble-metal systems under mild reaction conditions, offering cost-effective solutions for biomass-derived chemical production; (2) optimization of reaction systems, including a flow-type reaction system, which is much preferred in industry for scalability and cost efficiency; and (3) developing high stability catalysts is still a big challenge to meet the demands of industrial applications. Thus, future research on the catalytic conversion of HMF into valuable compounds should focus on designing efficient non-noble bimetallic catalysts, addressing catalyst stability and reaction system scalability challenges while optimizing the reaction parameters.

Author contributions

Xinluona Su: investigation, software, data curation, funding acquisition, and writing – original draft. Tingting Xiao: investigation, validation, and writing – original draft. Qihang Gong: investigation, software, and writing – original draft. Haiyang Cheng: supervision and writing – review and editing. Fengyu Zhao: supervision, conceptualization, funding acquisition, and writing – review and editing

Conflicts of interest

There are no conflicts of interest to declare.

Abbreviations

HMF	5-Hydroxymethylfurfural
BHMF	2,5-Bis(hydroxymethyl)furan
BHMTHF	2,5-Bis(hydroxymethyl)tetrahydrofuran
DMF	2,5-Dimethylfuran
DMTHF	2,5-Dimethyltetrahydrofuran
MF	5-Methylfurfural
MFA	5-Methylfurfuryl alcohol
1,2,6-HTO	1,2,6-Hexanetriol
1,2-HDO	1,2-Hexanediol
THF	Tetrahydrofuran
n-PrOH	n-Propanol
i-PrOH	i-Propanol
DIOX	1,4-Dioxane
EtOH	Ethanol
n-BuOH	n-Butanol
MeOH	Methanol
SMSI	Strong metal–support interaction
SO	Sodium oleate
HPS	Hollow polymeric sphere
HCS	Hollow carbon sphere
LDH	Layered double hydroxide
Ov	Oxygen vacancy

Data availability

No primary research results, software or code have been included and no new data were generated or analysed as part of this review.

Acknowledgements

References

1 W. Schutyser, T. Renders, S. Van den Bosch, S. F. Koelewijn, G. T. Beckham and B. F. Sels, *Chem. Soc. Rev.*, 2018, **47**, 852–908.

2 J. K. Saini, R. Saini and L. Tewari, *3 Biotech*, 2015, **5**, 337–353.

3 A. Demirbas, *Energy Convers. Manage.*, 2001, **42**, 1357–1378.

4 A. Tursi, *Biofuel Res. J.*, 2019, **6**, 962–979.

5 F. Sher, A. Yaqoob, F. Saeed, S. Zhang, Z. Jahan and J. J. Klemeš, *Energy*, 2020, **209**, 118444.

6 J. J. Bozell and G. R. Petersen, *Green Chem.*, 2010, **12**, 539.

7 P. Gallezot, *Chem. Soc. Rev.*, 2012, **41**, 1538–1558.

8 Q. Gong, P. Luo, J. Li, X. Su and H. Cheng, *Chemistry*, 2024, **6**, 941–961.

9 T. Kläusli, *Green Process. Synth.*, 2014, **3**, 235–236.

10 C. V. W. Fan, Y. Queneau and F. Popowycz, *Curr. Org. Synth.*, 2019, **16**, 583–614.

11 A. Cadu, K. Sekine, J. Mormul, D. M. Ohlmann, T. Schaub and A. S. K. Hashmi, *Green Chem.*, 2018, **20**, 3386–3393.

12 X. Liao, H. Cui, H. Luo, Y. Lv and P. Liu, *Chem. Eng. J.*, 2025, **505**, 159602.

13 M. M. Zhu, L. Tao, Q. Zhang, J. Dong, Y. M. Liu, H. Y. He and Y. Cao, *Green Chem.*, 2017, **19**, 3880–3887.

14 D. Zhao, T. Su, C. Len, R. Luque and Z. Yang, *Green Chem.*, 2022, **24**, 6782–6789.

15 K. S. Kozlov, L. V. Romashov and V. P. Ananikov, *Green Chem.*, 2019, **21**, 3464–3468.

16 M. M. Zhu, X. L. Du, Y. Zhao, B. B. Mei, Q. Zhang, F. F. Sun, Z. Jiang, Y. M. Liu, H. Y. He and Y. Cao, *ACS Catal.*, 2019, **9**, 6212–6222.

17 L. Hu, L. Lin and S. Liu, *Ind. Eng. Chem. Res.*, 2014, **53**, 9969–9978.

18 A. T. Hoang, A. Pandey, Z. Huang, R. Luque, K. H. Ng, A. M. Papadopoulos, W. H. Chen, S. Rajamohan, H. Hadiyanto, X. P. Nguyen and V. V. Pham, *ACS Sustainable Chem. Eng.*, 2022, **10**, 3079–3115.

19 R. Insyani, D. Verma, H. S. Cahyadi, S. M. Kim, S. K. Kim, N. Karanwal and J. Kim, *Appl. Catal., B*, 2019, **243**, 337–354.

20 M. D. Kumbhalkar, J. S. Buchanan, G. W. Huber and J. A. Dumesic, *ACS Catal.*, 2017, **7**, 5248–5256.

21 Y. Shao, J. Wang, K. Sun, G. Gao, M. Fan, C. Li, C. Ming, L. Zhang, S. Zhang and X. Hu, *ACS Appl. Nano Mater.*, 2022, **5**, 5882–5894.

22 B. Pomeroy, M. Grilc and B. Likozar, *Green Chem.*, 2021, **23**, 7996–8002.

23 R. Gautam, H. Li and S. Saravanamurugan, *ChemCatChem*, 2024, **16**, e202400691.

24 Z. Jiang, Y. Zeng, D. Hu, R. Guo, K. Yan and R. Luque, *Green Chem.*, 2023, **25**, 871–892.

25 A. A. Turkin, E. V. Makshina and B. F. Sels, *ChemSusChem*, 2022, **15**, e202200412.

26 Y. Wan and J. M. Lee, *ChemSusChem*, 2021, **15**, e202102041.

27 X. Wang, M. Arai, Q. Wu, C. Zhang and F. Zhao, *Green Chem.*, 2020, **22**, 8140–8168.

28 P. Mäki-Arvela, D. Ruiz and D. Y. Murzin, *ChemSusChem*, 2020, **14**, 150–168.

29 A. S. Chauhan, A. Kumar, R. Bains, M. Kumar and P. Das, *Biomass Bioenergy*, 2024, **185**, 107209.

30 J. Han, Y. H. Kim, H. S. Jang, S. Y. Hwang, J. Jegal, J. W. Kim and Y. S. Lee, *RSC Adv.*, 2016, **6**, 93394–93397.

31 F. Liu, M. Audemar, K. De Oliveira Vigier, J. M. Clacens, F. De Campo and F. Jérôme, *Green Chem.*, 2014, **16**, 4110–4114.

32 S. Zhang, H. Ma, Y. Sun, Y. Luo, X. Liu, M. Zhang, J. Gao and J. Xu, *Green Chem.*, 2019, **21**, 1702–1709.

33 S. Mhadmhan, A. Franco, A. Pineda, P. Reubroycharoen and R. Luque, *ACS Sustainable Chem. Eng.*, 2019, **7**, 14210–14216.

34 I. Elsayed, M. A. Jackson and E. B. Hassan, *ACS Sustainable Chem. Eng.*, 2020, **8**, 1774–1785.

35 Z. Zhang, S. Yao, C. Wang, M. Liu, F. Zhang, X. Hu, H. Chen, X. Gou, K. Chen, Y. Zhu, X. Lu, P. Ouyang and J. Fu, *J. Catal.*, 2019, **373**, 314–321.

36 Z. Chen, M. Lv, B. Kang, H. He, E. Du, Y. Chen and J. Zhang, *Appl. Catal., B*, 2025, **367**, 125078.

37 M. Lv, G. Chen, Y. Han, L. Huai, C. Chen, H. Yin and J. Zhang, *Appl. Catal., B*, 2025, **374**, 125405.

38 J. Tan, J. Cui, Y. Zhu, X. Cui, Y. Shi, W. Yan and Y. Zhao, *ACS Sustainable Chem. Eng.*, 2019, **7**, 10670–10678.

39 S. Nishimura, N. Ikeda and K. Ebitani, *Catal. Today*, 2014, **232**, 89–98.

40 F. Zhang, Y. Liu, F. Yuan, X. Niu and Y. Zhu, *Energy Fuels*, 2017, **31**, 6364–6373.

41 C. Sarkar, P. Koley, I. Shown, J. Lee, Y. F. Liao, K. An, J. Tardio, L. Nakka, K. H. Chen and J. Mondal, *ACS Sustainable Chem. Eng.*, 2019, **7**, 10349–10362.

42 S. Li, M. Dong, M. Peng, Q. Mei, Y. Wang, J. Yang, Y. Yang, B. Chen, S. Liu, D. Xiao, H. Liu, D. Ma and B. Han, *Innovation*, 2022, **3**, 100189.

43 B. Boro, P. Koley, A. Boruah, T. Hosseinnejad, J. M. Lee, C. C. Chang, C. W. Pao, S. Bhargava and J. Mondal, *ACS Sustainable Chem. Eng.*, 2024, **12**, 14200–14217.

44 X. Chen, J. Wang, Z. Du, H. Cai, Y. Huang, G. Chen, C. Tang and Y. Fang, *ChemistrySelect*, 2023, **8**, e202300862.

45 C. Liu, Y. Shi, Y. Shang, X. Wang, D. Liu, B. B. Mamba, A. T. Kuvarega and J. Gui, *Int. J. Quantum Chem.*, 2020, **121**, e26545.

46 B. Saha, C. M. Bohn and M. M. Abu-Omar, *ChemSusChem*, 2014, **7**, 3095–3101.

47 D. S. Pisal and G. D. Yadav, *Fuel*, 2021, **290**, 119947.

48 Y. Chen, H. Guo, J. Yang, K. Xu, X. Lu, Y. Yang, H. Lin, L. Wu, L. Tan, G. Yang, N. Tsubaki, X. Gu and Y. Tang, *Fuel*, 2024, **361**, 130682.

49 Y. Shang, C. Liu, Z. Zhang, S. Wang, C. Zhao, X. Yin, P. Zhang, D. Liu and J. Gui, *Ind. Eng. Chem. Res.*, 2020, **59**, 6532–6542.

50 W. Liao, Z. Zhu, N. Chen, T. Su, C. Deng, Y. Zhao, W. Ren and H. Lü, *Mol. Catal.*, 2020, **482**, 110756.

51 R. Guo, Y. Zeng, L. Lin, D. Hu, C. Lu, S. Conroy, S. Zhang, C. Zeng, H. Luo, Z. Jiang, X. Zhang, X. Tu and K. Yan, *Angew. Chem., Int. Ed.*, 2024, **64**, e202418234.

52 A. D. Talpade, M. S. Tiwari and G. D. Yadav, *Mol. Catal.*, 2019, **465**, 1–15.

53 B. Ledesma, J. Juárez, J. Mazarío, M. Domine and A. Beltramone, *Catal. Today*, 2021, **360**, 147–156.

54 X. Li, J. Wu, D. Cao and D. Cheng, *Ind. Eng. Chem. Res.*, 2024, **63**, 3880–3890.

55 J. Shi, M. Zhang, W. Du, W. Ning and Z. Hou, *Catal. Sci. Technol.*, 2015, **5**, 3108–3112.

56 J. Luo, H. Yun, A. V. Mironenko, K. Goulas, J. D. Lee, M. Monai, C. Wang, V. Vorotnikov, C. B. Murray, D. G. Vlachos, P. Fornasiero and R. J. Gorte, *ACS Catal.*, 2016, **6**, 4095–4104.

57 Z. Wen, S. Zhang, H. Yuan, Z. Zhang, J. She, Z. Qiao, Z. Liu, K. Liu, Z. Hu and C. Gao, *ACS Catal.*, 2024, **14**, 6305–6318.

58 X. Wang, Y. Liu and X. Liang, *Green Chem.*, 2018, **20**, 2894–2902.

59 M. Carmiel-Kostan, S. Nijem, S. Dery, G. Horesh and E. Gross, *J. Phys. Chem. C*, 2019, **123**, 30274–30282.

60 A. Srifa, M. Kalong, W. Praikaew, S. Ratchahat, W. Chaiwat, W. Koo-Amornpattana, W. Klysubun, W. Limphirat, S. Assabumrungrat and S. Kawi, *ChemCatChem*, 2024, **16**, e202301360.

61 G. H. Wang, J. Hilgert, F. H. Richter, F. Wang, H. J. Bongard, B. Spliethoff, C. Weidenthaler and F. Schüth, *Nat. Mater.*, 2014, **13**, 293–300.

62 H. Kataoka, D. Kosuge, K. Ogura, J. Ohyama and A. Satsuma, *Catal. Today*, 2020, **352**, 60–65.

63 G. Gao, Z. Jiang and C. Hu, *Front. Chem.*, 2021, **9**, 759512.

64 X. Xu, L. Lan, J. Xu, Z. Liang, J. Tan, H. Wang and S. Qiu, *Catal. Lett.*, 2024, **154**, 5152–5162.

65 Z. Huang, Y. Liu, L. Chen, X. Zhang, J. Liu, C. Wang, Q. Zhang and L. Ma, *Mol. Catal.*, 2024, **561**, 114169.

66 Y. Xin, S. Li, H. Wang, L. Chen, S. Li and Q. Liu, *Catalysts*, 2021, **11**, 915.

67 Y. Wang, Y. Wang, Y. Lu, Q. Cao and W. Fang, *Chem. Commun.*, 2021, **57**, 1742–1745.

68 Z. Dong, Y. Zhang and H. Xia, *RSC Adv.*, 2024, **14**, 14982–14991.

69 M. Esen, S. Akmaz, S. N. Koç and M. A. Gürkaynak, *J. Sol-Gel Sci. Technol.*, 2019, **91**, 664–672.

70 Z. Gao, G. Fan, M. Liu, L. Yang and F. Li, *Appl. Catal., B*, 2018, **237**, 649–659.

71 Y. Yang, Q. Liu, D. Li, J. Tan, Q. Zhang, C. Wang and L. Ma, *RSC Adv.*, 2017, **7**, 16311–16318.

72 A. M. Ruppert, M. Brzezińska and N. Keller, *Catal. Today*, 2024, **433**, 114651.

73 D. D. Lakshmi, Yogita, B. S. Rao and N. Lingaiah, *Sustainable Energy Fuels*, 2024, **8**, 43–53.

74 F. Zhang, H. Wu, Q. Wang, D. Li and J. Feng, *AlChE J.*, 2023, **70**, e18289.

75 S. Srivastava, G. C. Jadeja and J. Parikh, *Chin. J. Catal.*, 2017, **38**, 699–709.

76 X. Wang, C. Zhang, Z. Zhang, Y. Gai and Q. Li, *J. Colloid Interface Sci.*, 2022, **615**, 19–29.

77 B. Chen, F. Li, Z. Huang and G. Yuan, *Appl. Catal., B*, 2017, **200**, 192–199.

78 W. Zhao, X. Zhu, Z. Zeng, J. Lei, Z. Huang, Q. Xu, X. Liu and Y. Yang, *Mol. Catal.*, 2022, **524**, 112304.

79 Q. Zhang, J. Zuo, L. Wang, F. Peng, S. Chen and Z. Liu, *ACS Omega*, 2021, **6**, 10910–10920.

80 P. Hao, J. Zuo, W. Tong, J. Lin, Q. Wang and Z. Liu, *Front. Chem.*, 2022, **10**, 882670.

81 E. O. Kobzar, L. N. Stepanova, A. A. Nepomniashchii, A. V. Vasilevich, T. I. Gulyaeva, M. V. Trenikhin and A. V. Lavrenov, *Hydrogen*, 2023, **4**, 644–657.

82 D. Hu, H. Hu, H. Zhou, G. Li, C. Chen, J. Zhang, Y. Yang, Y. Hu, Y. Zhang and L. Wang, *Catal. Sci. Technol.*, 2018, **8**, 6091–6099.

83 L. L. K. S. Arias, A. Garcia-Ortiz, M. J. Climent, P. Concepcion, S. Iborra and A. Corma, *Catal. Sci. Technol.*, 2021, **11**, 3353–3363.

84 P. Aswin, A. C. Kothari, P. P. Neethu, R. Bal, N. J. Venkatesha, H.-L. Hsu, V. Ganesh and A. Sakthivel, *Catal. Lett.*, 2024, **154**, 4906–4917.

85 J. Luo, M. Monai, C. Wang, J. D. Lee, T. Duchoň, F. Dvořák, V. Matolín, C. B. Murray, P. Fornasiero and R. J. Gorte, *Catal. Sci. Technol.*, 2017, **7**, 1735–1743.

86 N. Viar, J. M. Requies, I. Agirre, A. Iriondo, C. García-Sancho and P. L. Arias, *Energy*, 2022, **255**, 124437.

87 S. Umasankar, P. Tamizhdurai, P. S. krishnan, S. Narayanan, V. L. Mangesh and K. Shanthi, *Biomass Bioenergy*, 2020, **143**, 105868.

88 D. Guo, J. Lai, F. Cheng, W. Zhao, H. Chen, H. Li, X. Liu, D. Yin and N. Yu, *Chem. Eng. J. Adv.*, 2021, **5**, 100081.

89 N. Viar, J. M. Requies, T. Tabanelli, F. Cavani, A. Bueno and M. O. Bengoechea, *Sustainable Chem. Environ.*, 2023, **4**, 100051.

90 B. Seemala, C. M. Cai, C. E. Wyman and P. Christopher, *ACS Catal.*, 2017, **7**, 4070–4082.

91 M. V. Morales, J. M. Conesa, A. J. Galvin, A. Guerrero-Ruiz and I. Rodríguez-Ramos, *Catal. Today*, 2023, **423**, 114021.

92 R. J. Chimentão, H. Oliva, V. Russo, J. Llorca, J. L. G. Fierro, P. Mäki-Arvela, D. Y. Murzin and D. Ruiz, *J. Phys. Chem. C*, 2021, **125**, 9657–9678.

93 M. Przydacz, M. Jędrzejczyk, J. Rogowski, D. Ihiawakrim, N. Keller and A. M. Ruppert, *Fuel*, 2024, **356**, 129606.

94 M. Przydacz, M. Jędrzejczyk, J. Rogowski, M. Szynkowska-Józwik and A. M. Ruppert, *Energies*, 2020, **13**, 4660.

95 Y. Yu, H. Liu, J. Zhang, H. Zhang, Y. Sun and L. Peng, *Renewable Energy*, 2023, **209**, 453–461.

96 M. Kalong, A. Srifa, S. Ratchahat, W. Koo-amornpattana, Y. Poo-arporn, W. Limphirat, P. Khemthong, S. Assabumrungrat, K. Tomishige and S. Kawi, *Sustainable Energy Fuels*, 2023, **7**, 934–948.

97 T. Cai, L. Yao, J. Fan and H. Peng, *J. Taiwan Inst. Chem. Eng.*, 2023, **146**, 104870.

98 Y. Zhang, A. Rezayan, K. Wang, J. Wang, C. C. Xu and R. Nie, *ACS Catal.*, 2022, **13**, 803–814.

99 W. Sun, F. Zhong, X. Ge, W. Chen, G. Qian, Y. Cao, X. Duan, X. Zhou and J. Zhang, *React. Chem. Eng.*, 2024, **9**, 1796–1804.

100 X. Kong, Y. Zhu, H. Zheng, Y. Zhu and Z. Fang, *ACS Sustainable Chem. Eng.*, 2017, **5**, 11280–11289.

101 Y. Li, R. Wang, B. Huang, L. Zhang, X. Ma, S. Zhang, Z. Zhu, H. Lü and K. Yang, *Appl. Surf. Sci.*, 2022, **604**, 154579.

102 Y. B. Huang, M. Y. Chen, L. Yan, Q. X. Guo and Y. Fu, *ChemSusChem*, 2014, **7**, 1068–1072.

103 J. J. Wiesfeld, M. Kim, K. Nakajima and E. J. M. Hensen, *Green Chem.*, 2020, **22**, 1229–1238.

104 Y. Liu, X. Shi, J. Hu, K. Liu, M. Zeng, Y. Hou and Z. Wei, *ChemSusChem*, 2022, **15**, e202200193.

105 N. Ma, Y. Song, F. Han, G. I. N. Waterhouse, Y. Li and S. Ai, *Catal. Lett.*, 2020, **151**, 517–525.

106 K. S. Arias, B. Hurtado, M. J. Climent, S. Iborra and A. Corma, *ChemPlusChem*, 2024, **89**, e202300643.

107 Y. Bao, W. Pu, Y. Zhang, Y. Xiao and Y. Liu, *J. Environ. Chem. Eng.*, 2024, **12**, 114914.

108 S. Yao, X. Wang, Y. Jiang, F. Wu, X. Chen and X. Mu, *ACS Sustainable Chem. Eng.*, 2013, **2**, 173–180.

109 K. Lu, Z. Tan, Y. Wang, J. Li, C.-L. Liu and W.-S. Dong, *Fuel*, 2024, **377**, 132686.

110 G. P. Lu, B. Wang, Y. Li, Y. Lin, J. Hu, Z. Chen and F. Chen, *Appl. Catal., A*, 2023, **661**, 119240.

111 A. Rezayan, D. Wu, Z. Zhang, X. Yang, R. Nie, T. Lu, J. Wang, X. Si, Y. Zhang and C. Xu, *Green Chem.*, 2025, **27**, 2578–2591.

112 Z. Zeng, Q. Tang, B. Wen, L. Luo, X. Liu, Q. Xu and W. Zhong, *J. Environ. Chem. Eng.*, 2024, **12**, 112190.

113 K. Lu, M. Cao, Y. Du, H. Huang, W. Xiang, G. Liu, J. Li, C.-L. Liu, N. Tsubaki and W.-S. Dong, *Mol. Catal.*, 2025, **572**, 114765.

114 S. Carenco, A. Tuxen, M. Chintapalli, E. Pach, C. Escudero, T. D. Ewers, P. Jiang, F. Borondics, G. Thornton, A. P. Alivisatos, H. Bluhm, J. Guo and M. Salmeron, *J. Phys. Chem. C*, 2013, **117**, 6259–6266.

115 A. S. Edelstein, V. G. Harris, D. R. Rolison, L. Kurihara, D. J. Smith, J. Perepezko and M. H. D. Bassani, *Appl. Phys. Lett.*, 1999, **74**, 3161–3163.

116 L. Li, X. Feng, Y. Nie, S. Chen, F. Shi, K. Xiong, W. Ding, X. Qi, J. Hu, Z. Wei, L.-J. Wan and M. Xia, *ACS Catal.*, 2015, **5**, 4825–4832.

117 K. Zhu, F. Shi, X. Zhu and W. Yang, *Nano Energy*, 2020, **73**, 104761.

118 D. Wu, W. Y. Hernández, S. Zhang, E. I. Vovk, X. Zhou, Y. Yang, A. Y. Khodakov and V. V. Ordomsky, *ACS Catal.*, 2019, **9**, 2940–2948.